

PACS numbers: 42.15.Fr; 42.66.Ct
DOI: 10.1070/QE2008v038n11ABEH013841

Human eye aberrations: 2. Development of a dynamic model of the human eye based on measurements

S.O. Galetskiy, T.Yu. Cherezova, A.V. Kudryashov

Abstract. **A human eye model based on a flexible semipassive bimorph mirror is proposed and experimentally realised. The model can be used for the real-time reproduction of human eye aberrations and their fluctuations. The accuracy of the reproduction of individual Zernike polynomials and of total eye aberrations of inspected patients is discussed.**

Keywords: *dynamic eye model, aberrations, wavefront*.

1. Introduction

It is known [1 – 4] that all the elements of the human eye, including the cornea, change their properties in time depending on accommodation, intraocular pressure, temperature, heartbeat, etc. The reasons for fluctuations of human eye aberrations have not been completely studied so far. They are caused most likely by changes in the eye accommodation produced by the tremor of ciliary muscles, intraocular optical elements, etc. The possibility of precise and fast measurements of eye aberrations and their fluctuations necessitates the development of dynamic mathematical and experimental eye models.

One of the first attempts to develop the experimental dynamic model belongs to Korean scientists [5]. They developed a lens with a variable focal distance. The lens consisted of two glass diaphragms, the space between them being filled with oil, and the curvature of surfaces being controlled by the oil pressure inside the vessel. In this way, a dynamic optical element with a variable surface, which could reproduce defocus, was realised.

Another dynamic model of the eye, which can reproduce, along with defocus, various aberrations such as astigmatism, coma and spherical aberrations, was proposed in paper [6]. The model consists of two lenses. Aberrations can be induced by changing the position of these lenses. The disadvantages of the model are that it cannot take into account higher-order aberrations inherent in the human eye and cannot change aberrations in the real time.

S.O. Galetskiy, T.Yu. Cherezova Department of Physics, M.V. Lomonosov Moscow State University, Vorob'evy gory, 119992 Moscow, Russia; galetskyi1986@mail.ru, cherezova@mail.ru;
A.V. Kudryashov Shatura Branch of the Moscow State Open University, ul. Sportivnaya 9, 140700 Shatura, Moscow region; e-mail: kud@activeoptics.ru

Received 6 March 2008
Kvantovaya Elektronika **38** (11) 1053 – 1058 (2008)
Translated by M.N. Sapozhnikov

The further development of the dynamic eye models resulted in the creation of a model [7] based on the use of a liquid-crystal lens. The model can reproduce a pseudorandom sequence of defocus amplitudes with a specified frequency (8.33 Hz). It was shown that during the reproduction of the specified defocus amplitude, a considerable spherical aberration appears which is caused by saturation effects in the liquid-crystal lens. A comparison of the generated sequences of amplitudes of defocus aberration and spherical aberration with the measured amplitudes of these aberrations for the real eye showed that the initial amplitude of the reproduced defocus and its dispersion coincided with their values for the real eye. At the same time, the dispersion and average amplitude of the spherical aberration considerably differed from their values measured for the real eye. In addition, the power spectra of time fluctuations of defocus and spherical aberration amplitudes differed from the corresponding spectra for the real eye.

Thus, the human eye models available now cannot reproduce the behaviour both of lower- and higher-order aberrations typical for the human eye. We proposed in our paper [8] for the first time a new imitator of eye aberrations, in which a flexible bimorph mirror is used. This imitator can reproduce very precisely variations in human eye aberrations. In this paper, we investigate our human eye model in more detail and present new results obtained during the development of this model.

2. Analysis of time fluctuations of human eye aberrations

Before discussing the reproduction quality of aberrations provided by the imitator, it is necessary to present the results of measurements of such aberrations for inspected patients.

To analyse the dynamic properties of the optical system of the eye, it is necessary first of all to measure aberrations at the frequency exceeding the characteristic frequency of their fluctuations. In the case of 'fast' measurements, the question arises about the image processing rate, which includes calculations of the centre of masses of focal spots, local tilts, and Zernike polynomial coefficients. The software package of our aberrometer [9] was optimised so that one image was processed for ~ 1 ms. Thus, after the optimisation of the program, the measurement rate was limited only by the parameters of our equipment, mainly by the response time of the camera used in experiments. Aberrations were measured for 5 s with an interval of 20 ms up to the fourth radial order inclusive (the number of Zernike

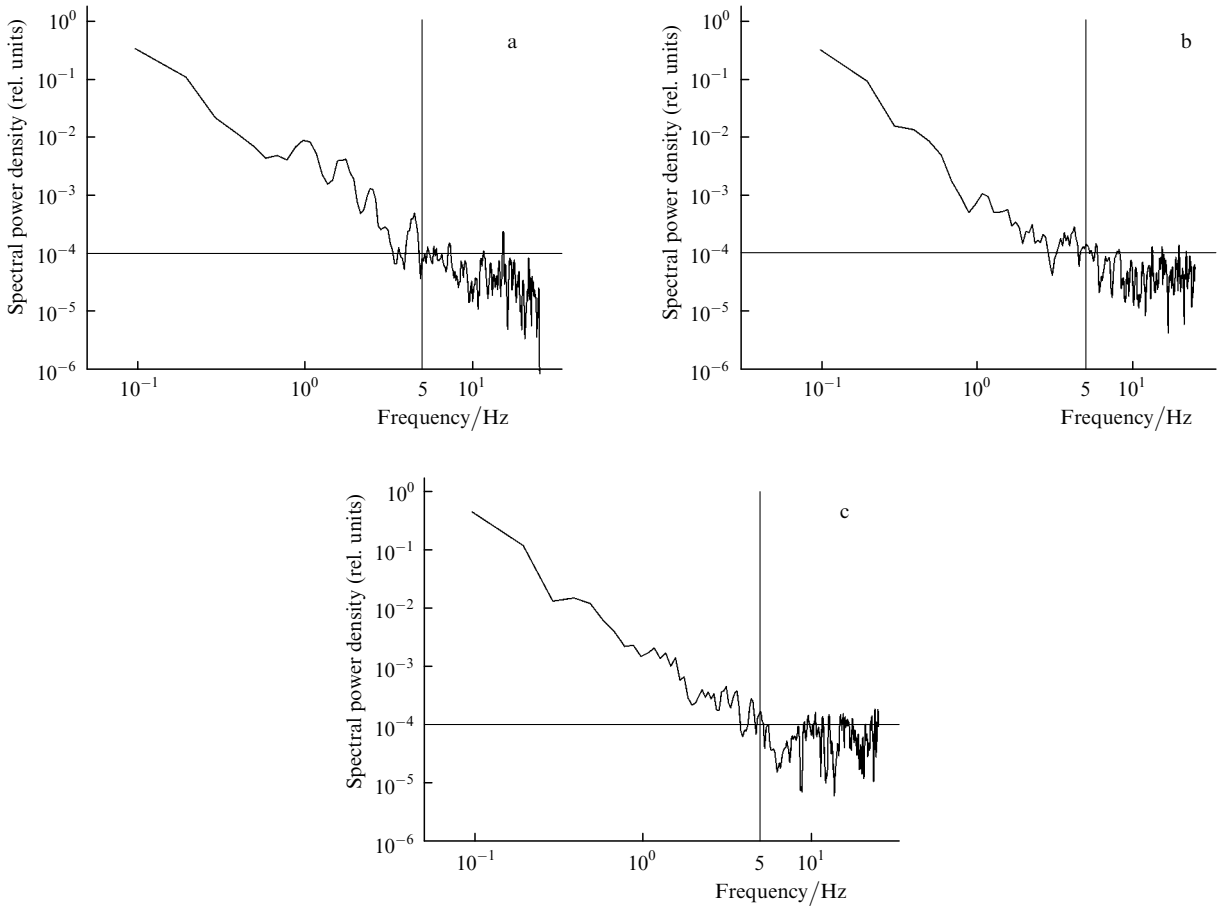

Figure 1. Normalised spectra of aberration fluctuations for patients BA (right eye) (a), GS (left eye) (b), and LR (left eye) (c). The horizontal straight line corresponds to the aberration measurement accuracy.

polynomial coefficients was $M = 14$). The measurement scheme is described in paper [10]. The measured time dependences of total aberrations were used to calculate the spectrum of fluctuation aberrations as the time Fourier transform of the root-mean-square deviation of the measured wavefront from the plane one.

Figure 1 presents the spectra of time fluctuations obtained for inspected patients. One can see that the spectral power density of fluctuations of eye aberrations at frequency 5 Hz decreases approximately by four orders of magnitude. Taking into account the aberration measurement accuracy (the root-mean-square deviation is $\lambda/10$), fluctuations with the spectrum lying above 5 Hz cannot be measured in fact. Therefore, a dynamic model should reproduce eye aberrations in the frequency range up to 5 Hz.

3. Optical scheme of the dynamical eye model

The main element of our dynamical eye model is a flexible semipassive bimorph mirror [11, 12]. The optical scheme of the model presented in Fig. 2 consists of a telescopic system of lenses T1 and T2, expanding a beam up to the mirror diameter, and of a flexible corrector of diameter 36 mm controlled with a special CDM-17-300V unit. The control unit is connected via the USB interface with a computer, which controls the mirror in real time with the help of the specialised software. The frequency of the first resonance of the bimorph mirror used to reproduce aberrations exceeded 1 kHz. Therefore, this corrector can provide the real-time reproduction of eye aberrations. Figure 3 shows the arrangement of controlling electrodes and the mirror photograph. This mirror is convenient for simulations of monochromatic aberrations of the human eye because it

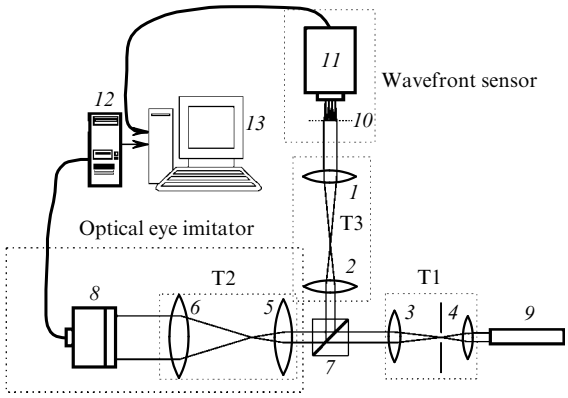

Figure 2. Experimental scheme of the model of the optical eye imitator: (*1*) ($f = 20$ mm), (*2*) ($f = 20$ mm), (*3*) ($f = 50$ mm), (*4*) ($f = 20$ mm), (*5*) ($f = 20$ mm), (*6*) ($f = 180$ mm) converging lenses; (*7*) beamsplitter cube (10×10 mm, 50/50); (*8*) bimorph mirror (18 electrodes, diameter 36 mm); (*9*) 780-nm, 2-mW LM-780-2AB diode laser (beam diameter 0.8 mm); (*10*) lens raster (20×20 microlenses of diameter 0.3 mm, $f = 8$ mm); (*11*) 50-Hz Basler A602f CCD camera; (*12*) CDM-17-300V mirror control unit; (*13*) computer; (T1 – T3) telescopes.

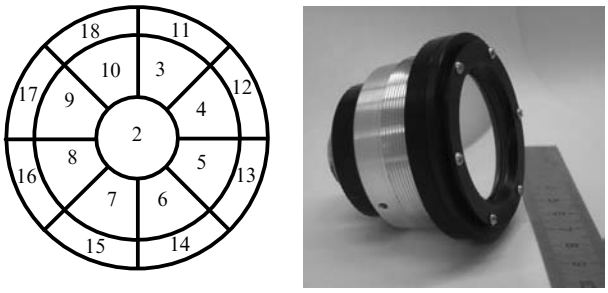

a b

Figure 3. Layout of electrodes (a) and the photograph of a bimorph mirror (b).

provides the maximum amplitude of the phase modulation (up to 10 μm from the maximum to minimum), the fast response, and the high accuracy of the reproduction of the specified wavefront profile (which are experimentally determined below).

To calculate the voltages applied to corrector electrodes, directly before the experiment the response functions for each of the control electrodes were measured. The response functions for the second (at the applied voltage +70 V), tenth, and fourteenth electrodes (+150 V) are presented in Fig. 4. The measured response functions were represented in the form of the matrix $\hat{R}$, whose element with subscripts i and j corresponds to the local tilt of the wavefront within the jth subaperture of the microlens raster of the Shack–Hartmann sensor (used for measurements of the response function) caused by a voltage of 1 V applied to the ith electrode; $\boldsymbol{m} = \hat{R}\boldsymbol{V}$. Here, $\boldsymbol{m}$ is the vector of local tilts of the wavefront and $\boldsymbol{V}$ is the voltage vector on electrodes. The feedback between these quantities is determined by the method of least squares:

$$\boldsymbol{V} = \left(\hat{R}^{\mathrm{T}}\hat{R}\right)^{-1}\hat{R}^{\mathrm{T}}\boldsymbol{m}. \tag{1}$$

One can see from Fig. 1 that the spectrum of time aberrations of the eye is bounded above by frequency 5 Hz. It follows from the Nyquist theorem that to provide the precise reproduction of all frequencies, it is necessary to specify the wavefront with the doubled frequency, i.e. with the frequency 10 Hz. For this purpose, we measured eye aberrations at the moment t_l ($t_l - t_{l-1} = 100$ ms). Aberrations were reproduced by calculating the local tilt vector $\boldsymbol{m}_l$ corresponding to eye aberrations measured at the instant t_l. The vector $\boldsymbol{m}^*_{l-1}$ of the local tilts of aberrations reproduced by the mirror at instant t_{l-1} was measured with the Hartmann sensor. Then, the difference $\Delta\boldsymbol{m}_l = \boldsymbol{m}_l - \boldsymbol{m}^*_{l-1}$ was calculated. Based on expression (1), the voltage vector applied to electrodes at the step l was calculated by the expression

$$\boldsymbol{V}_l = \boldsymbol{V}_{l-1} + \left(\hat{R}^{\mathrm{T}}\hat{R}\right)^{-1}\hat{R}^{\mathrm{T}}\Delta\boldsymbol{m}_l. \tag{2}$$

Here, $\boldsymbol{V}_{l-1}$ is the voltage vector applied at the previous step (at the instant t_{l-1}). Thus, expression (2) shows that the control algorithm is a modification of the classical phase conjugation scheme generalised to the case when the required convergence limit of a closed loop changes in time.

Figure 5 demonstrates good reproduction of human eye aberrations by the artificial eye model. Here, the time fluctuations of aberrations corresponding to the eyes of three patients are presented. The reproduction quality of the aberration amplitude was estimated from the residual error

$$e(t) = \left(\sum_{n=1}^{M}[z_n(t) - Z_n(t)]^2\right)^{1/2}, \tag{3}$$

where $z_n(t)$ are Zernike polynomial coefficients reproduced by the mirror and $Z_n(t)$ are Zernike polynomial coefficients characterising patient's eye aberrations at the corresponding instants.

Table 1 presents time-averaged errors in the reproduction of aberrations for eight eyes (the averaging time was 10 s). The correlation coefficient between measured and reproduced aberrations is also shown. The correlation coefficient was calculated by using the root-mean-square deviations of the wavefront from a plane wavefront at different time intervals as random-value realisations. The correlation coefficient α was calculated by the expression

$$\alpha = \frac{\langle(\sigma_{\mathrm{m}} - \langle\sigma_{\mathrm{m}}\rangle)(\sigma_{\mathrm{p}} - \langle\sigma_{\mathrm{p}}\rangle)\rangle}{(D_{\mathrm{m}}D_{\mathrm{p}})^{1/2}}, \tag{4}$$

where σ_{m} is the root-mean-square deviation of the measured wavefront from a plane wavefront; σ_{p} is the root-mean-square deviation of the reproduced wavefront from a plane wavefront; D_{m} is the dispersion of σ_{m}; and D_{p} is the dispersion of σ_{p}. The angle brackets mean averaging in time (100 measurements for 10 s).

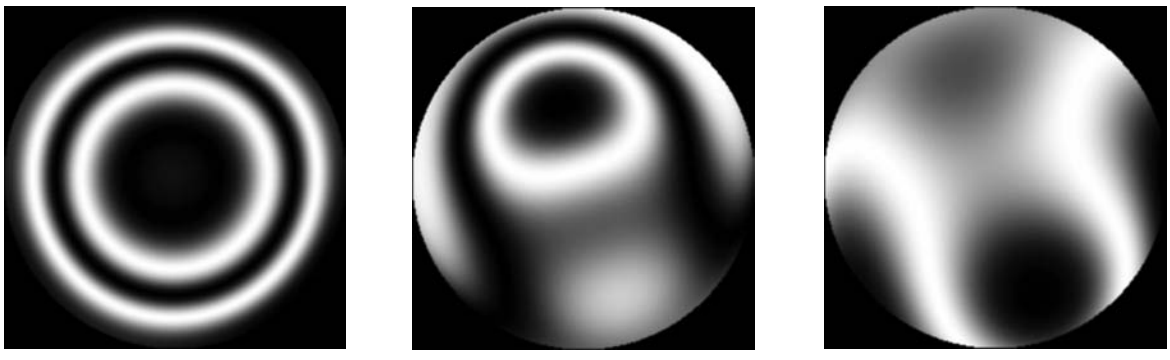

a b c

Figure 4. Response functions of the mirror for the second (a), tenth (b), and fourteenth (c) electrodes.

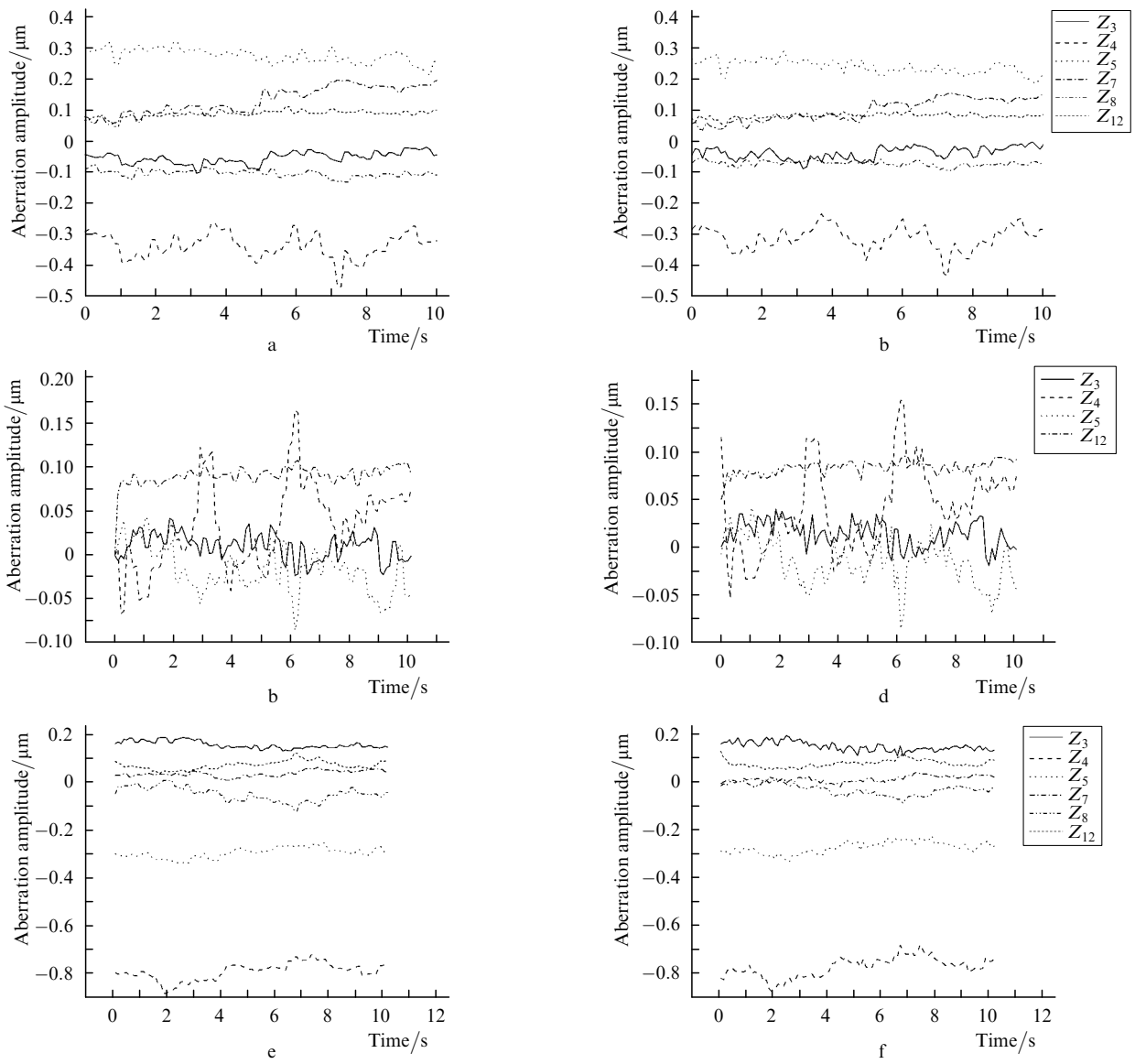

Figure 5. Amplitudes of aberrations measured (a, c, e) and reproduced with the help of the dynamic eye model (b, d, f) for patients BA (left eye) (a, b), GS (left eye), and LR (right eye) (e, f).

Table 1. Average reproduction error $\langle e \rangle$ of eye aberrations and correlation coefficient α.

Patient	$\langle e \rangle$/μm	α
GS (left eye)	0.03	0.86
GS (right eye)	0.04	0.99
DA (left eye)	0.06	0.98
DA (right eye)	0.07	0.94
BA (left eye)	0.08	0.94
BA (right eye)	0.04	0.92
LR (left eye)	0.11	0.87
LR (right eye)	0.06	0.97

One can see from Table 1 that the reproduction quality of different aberrations can be somewhat different for different patients, which is related to the different amplitude and structure of the phase distortions being reproduced. However, the error for seven from the eight reproduced phase profiles does not exceed $\lambda/10$. The relatively large error for patient LR (left eye) is probably caused by the rather large amplitude of his eye aberrations (4.8 μm) and also by the non-optimal configuration of the electrodes of the mirror used for the reproduction of specific aberrations of this eye.

Figure 6 presents the distribution of the total reproduction error by individual Zernike polynomials (the error was calculated by the expression $e_n = \langle [z_n(t) - Z_n(t)]^2 \rangle^{1/2}$. One can see that all aberrations are reproduced with the error smaller than $\lambda/20$ (0.039 μm). Figure 7 shows the time dependence of the residual error of the wavefront reproduction [see expression (3)].

We analysed the dynamic characteristics of the model by calculating the spectrum of total aberrations reproduced by it. Figure 8 presents the spectra of fluctuations of eye aberrations for three patients together with the spectra of aberrations reproduced by the eye imitator. One can see that these spectra almost completely coincide, demonstrating the high reproduction quality of the dynamics of aberrations by our model.

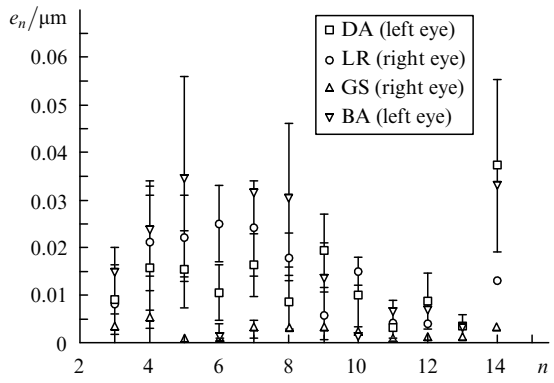

Figure 6. Average reproduction error for different Zernike polynomials for four patients (n is the polynomial number).

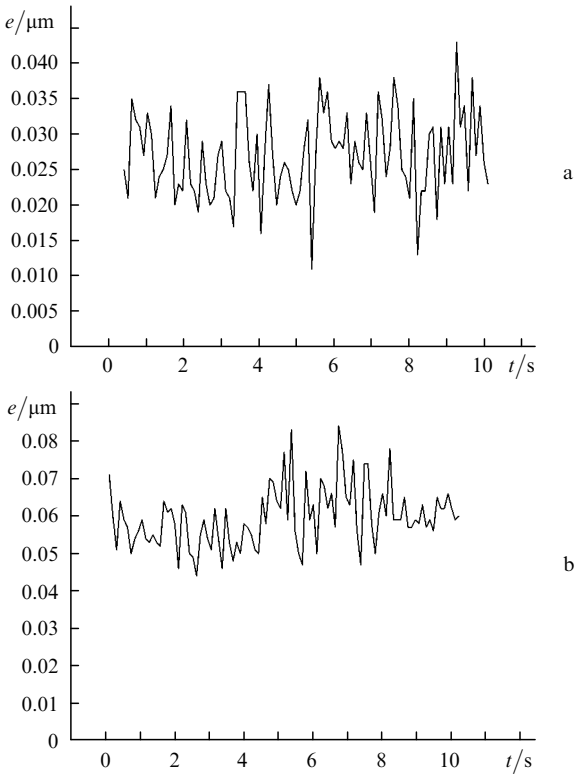

Figure 7. Time dependences of the wavefront reproduction error for patients GS (left eye) (a) and LR (right eye) (b).

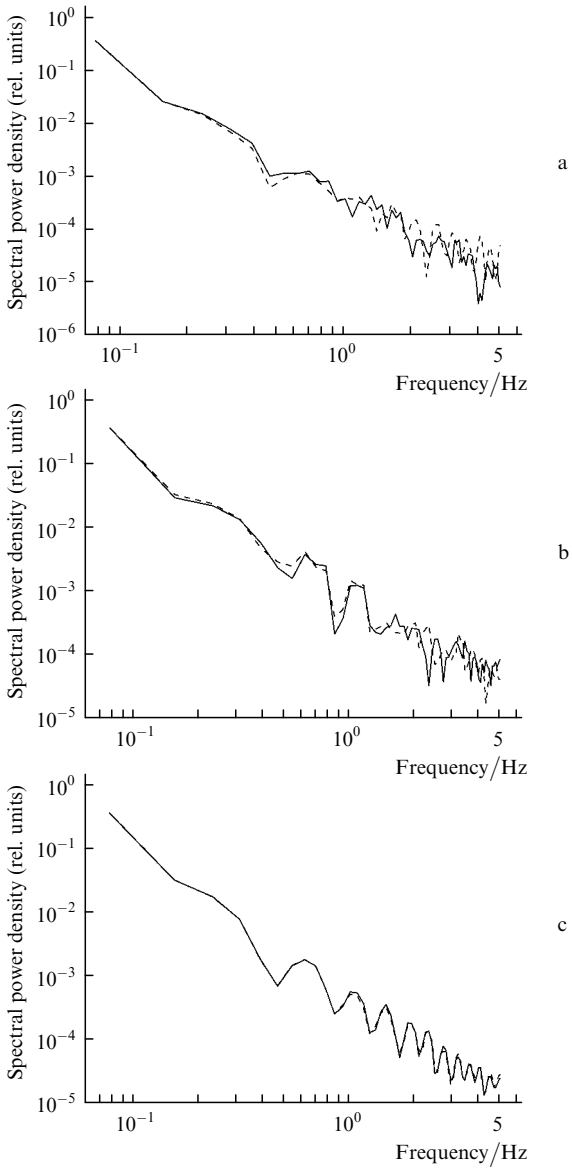

Figure 8. Normalised fluctuation spectra for measured aberrations (dashed curves) and aberrations reproduced by the eye imitator (solid curves) for patients BA (right eye) (a), GS (left eye) (b), and LR (left eye) (c).

4. Compensation of aberrations

We used the dynamic eye model developed here not only for the reproduction but also for compensation of eye aberration in real time. For this purpose, the model was introduced to the optical system of the aberrometer so that the mirror surface was conjugated with the patient pupil. The mirror was controlled by the phase conjugation method. The system operated in a closed loop at frequency 10 Hz (the iteration time was 100 ms). We studied the compensation quality of eye aberrations for several patients in terms of the residual root-mean-square error, the Strehl ratio, and the modulation transfer function. The pupil size was 4 mm in all cases.

Figure 9 presents the interferograms of the wavefront of radiation scattered by the eye retina calculated without or with correction for aberrations. Figure 10 presents the root-mean-square deviations of the wavefront averaged for the measurement time (10 s), which were obtained without correction and with correction for four patients, and the corresponding Strehl ratios. The residual correction error

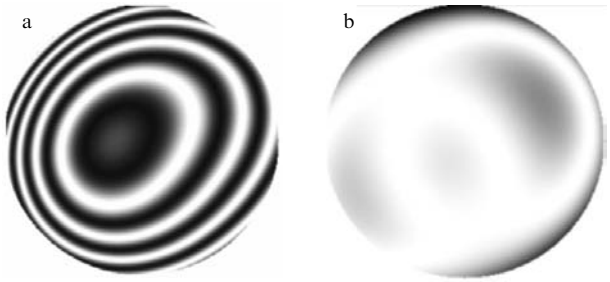

Figure 9. Interferograms calculated from the measured aberrations of the left eye of patient LR without compensation (a) and with compensation (b).

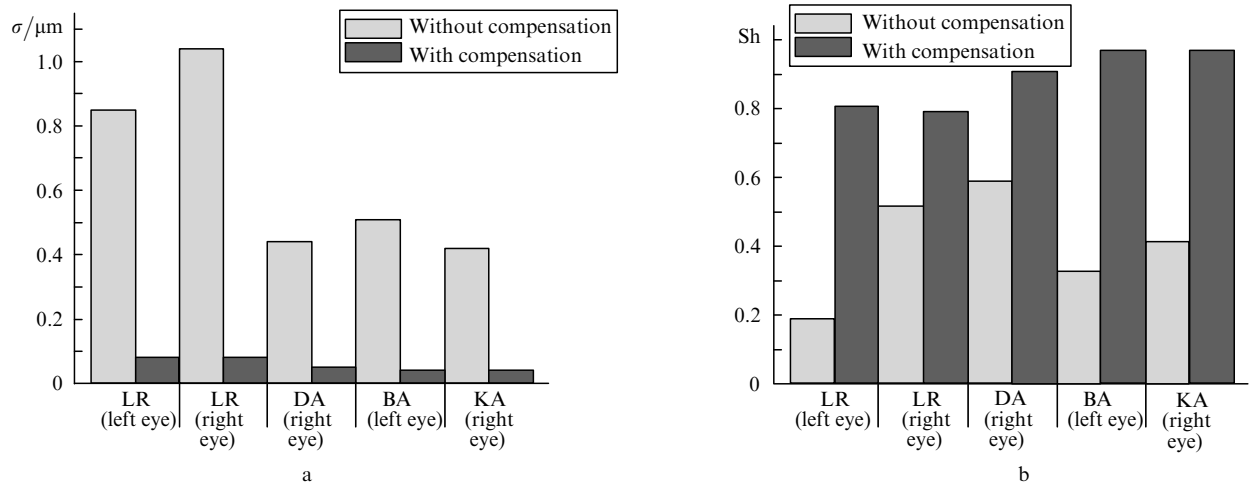

Figure 10. Root-mean-square deviation σ (a) and the Strehl ratio Sh (b) for different patients.

for all patients was $\lambda/10$ or smaller. In this case, the root-mean-square deviation was more than 10 times smaller. It is natural that the dynamic adaptive correction also results in the increase in the Strehl number, which increased up to 0.8 and more for all inspected patients and exceeded 0.9 in three cases. We studied the influence of correction on the spatial resolution by calculating the modulation transfer functions. Figure 11 shows these functions for a diffraction-limited system and also for the optical system of the left eye of patient LR without and with correction. It is obvious that the values of the function increase in the entire frequency region after correction, approaching the values corresponding to a diffraction-limited system, while the limiting spatial resolution increases.

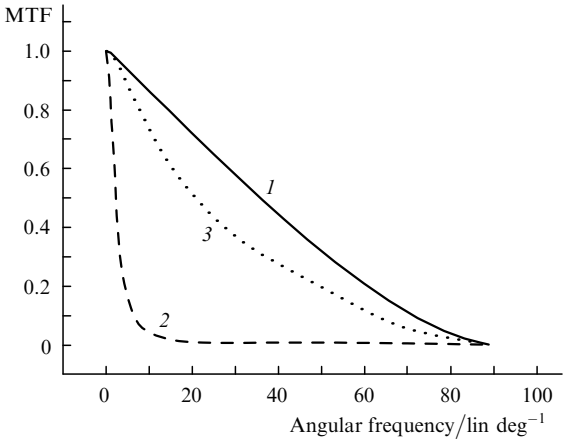

Figure 11. Modulation transfer unction (MTF) for a diffraction-limited system (*1*) and the optical system of the left eye of patient LR without compensation (*2*) and with compensation (*3*).

5. Conclusions

The eye model proposed in our paper, which is in fact a dynamic generator of monochromatic eye aberrations, allows one to reproduce and change dynamically higher-order aberrations with an error smaller than $\lambda/20$ ($\lambda =$ 780 nm). This model can be used to calibrate ophthalmologic instruments and elements correcting vision, for example, spectacles, contact, and intraocular lenses. This model can reproduce completely the temporal spectrum of human eye aberrations in the frequency range up to 5 Hz, their short-time fluctuations, changes in the aberration amplitude due to accommodation, fatigue, etc. with an error of $\lambda/10$ for different patients. The experimental model developed in the paper can be used to perform complete diagnostic studies of the eye. At present, this system is integrated into the optical scheme of an aberrometer and can be used to compensate for eye aberrations in real time with the residual error smaller than $\lambda/10$.

References

1. Hofer H., Artal P., Singer B., Aragon J.L., Williams D.R. *J. Opt. Soc. Am. A*, **18**, 497 (2001).
2. Diaz-Santana L., Torti C., Munro I., Gasson P., Dainty C. *Opt. Express*, **11**, 2597 (2003).
3. Hampson K.M., Paterson C., Dainty C., Mallen E.A.H. *J. Opt. Soc. Am. A*, **23**, 1082 (2006).
4. Hampson K.M., Munro I., Paterson C., Dainty C. *J. Opt. Soc. Am. A*, **22**, 1241 (2005).
5. Ahn S.-H., Kim Y.-K. *Sensors Actuators A: Physical*, **78**, 48 (1999).
6. Sheehy J., Gish K., Kenneth W., Sprenger J. US Patent 6485142 (2002).
7. Fernandez E.J., Artal P. *Appl. Opt.*, **46**, 6971 (2007).
8. Galetskiy S.O., Belyakov A.I., Cherezova T.Yu., Kudryashov A.V. *Opt. Zh.*, **73**, 79 (2006).
9. Galetskiy S., Letfullin R., Dubinin A., Cherezova T., Belyakov A., Kudryashov A. *Proc. SPIE Int. Soc. Opt. Eng.*, **6018**, 601806 (2005).
10. Dubinin A.V., Cherezova T.Yu., Kudryashov A.V. *Kvantovaya Elektron.*, **38**, 1048 (2008) [*Quantum Electron.*, **38**, 1048 (2008)].
11. Kudryashov A.V., Samarkin V.V. *Opt. Commun.*, **118**, 317 (1995).
12. Kaptsov L.N., Kudryashov A.V., Samarkin V.V., Seliverstov A.V. *Kvantovaya Elektron.*, **19**, 579 (1992) [*Quantum Electron.*, **22**, 533 (1992)].